

# Dynamic Aware: Adaptive Multi-Modal Out-of-Distribution Detection for Trajectory Prediction in Autonomous Vehicles

Tongfei Guo<sup>1</sup> and Lili Su<sup>1</sup>

**Abstract**—Trustworthy trajectory prediction is central to autonomous vehicle (AV) safety in real-world traffic. In deployment, prediction models inevitably face distribution shifts between training data and real-world conditions, where rare traffic scenes and environmental uncertainties induce out-of-distribution (OOD) scenarios. While prior OOD detection in AVs focuses on perception, trajectory-level detection remains underexplored. Recent work frames this task as a quickest change detection problem, which offers a principled trade-off between detection delay and false alarms [1]. The resulting CUSUM algorithms are lightweight and model-agnostic, making them attractive for onboard deployment. However, despite this progress, existing methods largely overlook a key aspect of temporal dynamics. Our analysis of real-world benchmarks reveals that prediction errors are often *multi-modal*, exhibiting distinct low- and high-error modes that evolve with open-world driving context. Observing this, we propose *Mode-Aware CUSUM*, which explicitly models multiple error regimes while retaining the efficiency and general compatibility of classical CUSUM. By dynamically identifying the active error mode and adapting detection thresholds, our method enables robust monitoring across heterogeneous conditions. Experiments on large-scale trajectory benchmarks demonstrate consistent reductions in detection delay and false alarms.

## I. INTRODUCTION

Trajectory prediction is vital for autonomous vehicle (AV) safety, but models often struggle with distribution shifts between training and real-world deployment. While large-scale datasets capture routine driving, they underrepresent rare “tail” scenes that contain elements like aggressive maneuvers or complex roundabouts. Furthermore, real-world traffic often suffers from a wide range of uncertainties, such as irregular road blockages and extreme weathers. These out-of-distribution (OOD) scenarios often lead models to generate overconfident but hazardous forecasts that may ultimately mislead the decision-making of the ego vehicles.

Existing research on OOD detection in AVs has primarily focused on traditional computer vision tasks such as object detection and semantic segmentation [2], [3], with representative approaches including post-hoc scoring and energy-based models [4], [5].

These methods are predominantly frame-wise. A key limitation of this frame-wise approach is that it determines whether the ego vehicle is in an in-distribution (ID) or OOD traffic scene solely based on information from the current frame, thereby overlooking the spatiotemporal correlations

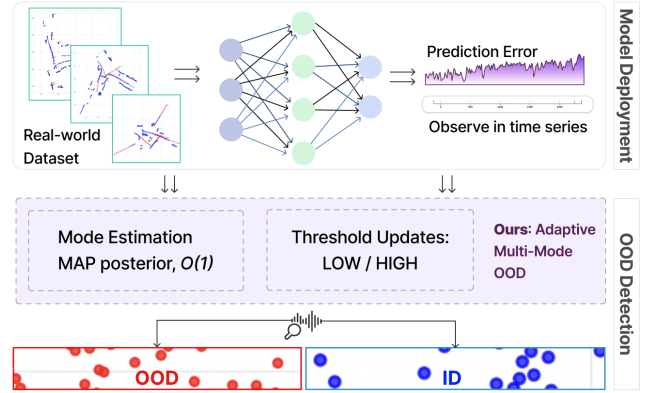


**Fig. 1: Illustration of our adaptive multi-mode OOD detection framework for trajectory prediction in AVs.** The framework monitors prediction errors in real-time, dynamically identifies the active error regime (low-error or high-error mode), and adapts detection thresholds accordingly.

among the trajectories of surrounding agents. As a consequence, frame-wise approaches tend to perform well only when the distance between ID and OOD data is sufficiently large, resulting in significantly suboptimal detection performance in the more challenging yet practical setting where the deviations between OOD and ID scenes are minor at individual frames but may gradually escalate into hazardous situations if left unnoticed. Such cases are referred to as **deceptive OOD scenarios** [1], which are the focus of this paper.

While uncertainty quantification (UQ) could help guide OOD detection [6], [7], existing methods mostly lack theoretical guarantees. Observing the sequential nature of traffic, a recent work framed trajectory OOD detection as a quickest change detection problem [1]. They extended the *light-weight* cumulative sum (CUSUM) method for trajectory prediction, which can provide formal guarantees on the trade-off between detection delay and false alarms under comparable or more relaxed probabilistic assumptions than UQ. Moreover, these methods are agnostic to the specific models deployed, making them flexible and general.

Despite this progress, existing methods [1] largely overlook a key aspect in AV applications – the evolution of the error distribution. Our empirical analysis across multiple real-world benchmarks shows that prediction errors consistently exhibit a *multi-modal* distribution with the active mode evolving over time; details can be found in Section III. Ignoring the dynamics of error modes is not only theoretically unsound but also leads to degraded practical performance.

\*This work was not supported by any organization

<sup>1</sup>Department of Electrical and Computer Engineering, Northeastern University, Boston, MA, USA. {guo.t, l.su}@northeastern.edu

For instance, consider a scenario in which the ego vehicle is driving on a lightly trafficked, mostly straight road. Relying on global statistics used in [1] as the detection input may result in improperly calibrated high thresholds, leading to prolonged detection delays that could compromise safety. Building awareness to the error mode dynamics is nontrivial. As illustrated in Section III, the naïve scene-level statistics—such as agent counts, maximum/average speeds, or map snapshots—offer direct cues for identifying mode transitions.

In this paper, we propose an adaptive QCD framework that tracks the error modes and adjusts detection thresholds dynamically. Our method preserves CUSUM’s efficiency and analytical rigor while adding lightweight mode estimation for threshold adaptation. Our framework requires only streaming prediction residuals—no model internals, ground-truth labels, or expensive uncertainty quantification.

**Contributions.** Our contributions can be summarized as:

- We provide the first systematic evidence, across multiple widely-used trajectory prediction benchmarks, that prediction errors exhibit *multi-modal* distributions, and the active mode evolves over time.
- We introduce a *Mode-Aware CUSUM* (MA-CUSUM) algorithm that adapts detection thresholds based on the estimated error mode.
- We conduct extensive experiments on established benchmarks (ApolloScape, NGSIM, nuScenes), demonstrating that MA-CUSUM consistently achieves faster detection with smaller false alarm rates than non-adaptive baselines, while outperforming existing UQ- and vision-based OOD methods at lower computational cost.
- Our design is modular and compatible with diverse prediction models and error distributions, requiring only prediction residuals as input. Computationally, our method only introduces a one-timestamp delay beyond the inherent detection delay, making it practical for real-time use.

## II. RELATED WORK

**Trajectory Prediction.** Trajectory prediction is a critical component in autonomous driving. Early approaches relied on recurrent neural networks [8] to model single-agent behavior, while subsequent work introduced interaction-aware mechanisms such as social pooling and graph-based models to capture multi-agent dependencies [9]. More recently, advanced methods have increasingly adopted Transformer architectures [10] and spatio-temporal graph neural networks [11] to improve accuracy, enable real-time forecasting, and capture complex interactions. Despite these advances, the reliability of trajectory prediction under distribution shifts remains underexplored. A small number of studies address related issues through uncertainty estimation [12] and adversarial attacks [13]. Robustness to OOD samples is increasingly recognized as a fundamental performance indicator for trajectory prediction models [14]. However, comprehensive approaches for OOD detection in trajectory prediction remain underexplored.

**OOD Detection in AVs.** Existing OOD detection research in AVs has primarily focused on perception tasks such as object

detection, semantic segmentation, and depth estimation [2], [3]. Representative approaches include scoring functions such as maximum softmax probability (MSP) [4] and energy-based scores [5], as well as latent-space density estimation techniques [15]. These OOD detection methods are not fully suited for trajectory prediction since they overlook the spatiotemporal correlations among the trajectories of surrounding agents. Moreover, as summarized in [16], prevailing OOD performance metrics often prioritize recognition accuracy without addressing detection delay and computation complexity. In AV practice, short detection delay is critical for enabling timely control adaptation, while low computational complexity is necessary to satisfy on-board resource constraints.

**Application of UQ to OOD Detection.** Popular UQ for trajectory prediction [6], [7] include deep ensembles, Monte Carlo dropout, and Bayesian neural networks. While effective, these methods typically incur substantial computational overhead. Recent research has focused on developing more efficient UQ frameworks tailored for OOD detection. For instance, [12] introduced a scalable approach that models ID samples within a latent space using a Gaussian Mixture Model (GMM), identifying OOD samples as low-likelihood outliers—a principle shared by other density-based detection methods [15], [17]. Complementarily, [1] introduced an external monitoring module that operates directly on model outputs, detecting OOD samples via prediction error statistics without altering the underlying predictor.

**Quickest Change-Point Detection (QCD).** QCD provides a rigorous framework for monitoring sequential data to identify the *change-point* at which its underlying distribution shifts, with the dual objectives of minimizing the detection delay and controlling the frequency of false alarms [18]. This formalism, with applications spanning finance, climatology, and network monitoring [19], is typically pursued within either a Bayesian [20] or minimax setting. In particular, CUSUM algorithm is first-order asymptotically optimal [21], [22], [18]. These strong theoretical guarantees, combined with its computational efficiency, make CUSUM a powerful and principled foundation for our work.

## III. MODE-DEPENDENT ERROR DISTRIBUTIONS

Our empirical analysis across multiple representative real-world benchmarks shows that: prediction errors consistently exhibit *multi-modal* distributions whose active mode evolves over time. We conjecture that this multi-modality behavior is not dataset-specific but generalizes to a broader spectrum of trajectory prediction models and datasets. Moreover, the set of modes may extend beyond two, potentially encompassing a richer class of error regimes.

### A. Overall Multiple Error Modes

We begin with an empirical study of prediction errors across multiple models (e.g., GRIP++ [24], FQA [25]) and datasets (ApolloScape [26], NGSIM [27], nuScenes [28]). The datasets vary in map topology, traffic composition, and density; details can be found in Section VI-A.

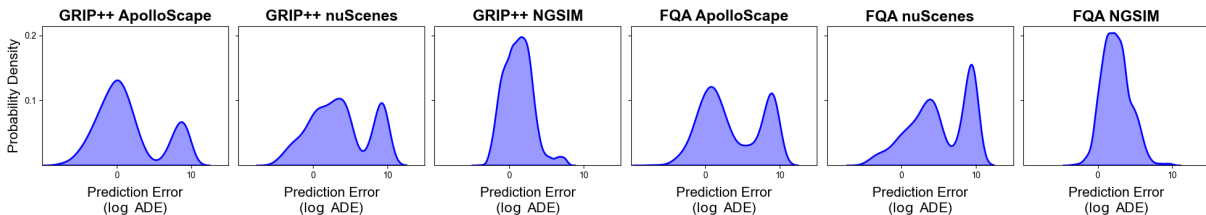


**Fig. 2: Multi-modal distributions of prediction errors.** The  $x$ -axis denotes prediction error (log-scale ADE; see Section IV-D), and the  $y$ -axis denotes probability density. Plots were averaged over 500 independent runs, the empirical distribution consistently exhibits a bi-modal structure, well approximated by a two-component GMM. The lower-error component is defined as the *low-risk mode*, while the higher-error component represents the *high-risk mode*.

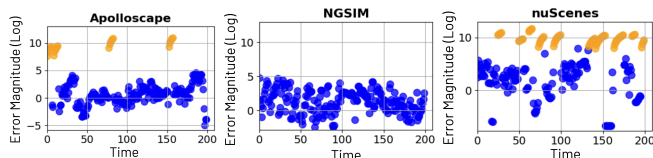


**Fig. 3: Mode dynamics across different driving scenes (FQA model).** Datasets: *ApolloScape* (left), *NGSIM* (center), *nuScenes* (right). The  $x$ -axis represents the time frame indices; the  $y$ -axis is error magnitude (log scale). The modes were inferred by the classic MAP estimation via the GMM posterior (blue = low-risk, orange = high-risk) [23].

As illustrated in Fig. 2, the overall prediction errors for each of the datasets are well approximated by a Gaussian Mixture Model (GMM) that naturally divides into two latent components: a *low-risk mode* component and a *high-risk mode* component. Table I reports the GMM mode weights across all model–dataset combinations. The high-risk mode proportion varies substantially—from 5.9% to 42.3%—reflecting the diversity of driving contexts and models.

### B. On the Temporal Evolution of Error Modes

We observe that the error modes evolve over time, potentially following different dynamics across datasets. Intuitively, in highway driving, the ego vehicle often remains in the same error mode for extended periods with occasional transitions, whereas dense urban intersections feature more abrupt and frequent behavioral changes, resulting in frequent mode switches. Our experimental results align with this intuition, as is shown in Fig. 3:

- **ApolloScape and nuScenes:** Urban intersection settings in which close-proximity interactions drive frequent and abrupt mode shifts.
- **NGSIM:** Highway settings in which prediction errors predominantly remain in the low-risk mode, with occasional high-risk episodes corresponding to maneuvers such as lane changes or merging.

The mode dynamics under GRIP++ are expected to be somewhat similar to those in Fig. 3 yet with overall lower frequency in high-risk mode in *ApolloScape* and *nuScenes*.

### C. Latent Modes are Not Directly Observable

Due to the inherent randomness of prediction errors, the underlying error mode is often latent and not directly observable from visual inputs. Readily available scene-level statistics—such as agent counts, maximum/average speeds, or

**TABLE I: GMM mode weights (%).**

	ApolloScape	nuScenes	NGSIM
GRIP++	77.5/22.5	67.4/32.6	94.1/5.9
FQA	57.7/42.3	60.2/39.8	80.8/19.2

Low-risk/high-risk.

map snapshots—offer no reliable cues for identifying mode transitions.

As shown in Fig. 4, mode transitions (highlighted by dashed pink lines) occur without significant corresponding changes in observable metrics: agent density remains stable, speed metrics show no anomalous patterns, and scene snapshots display consistent visual characteristics. The weak correspondence between observable scene information and error modes limits the effectiveness of purely vision-based approaches for mode identification, thereby motivating our statistics-based mode estimation framework.

## IV. PROBLEM FORMULATION: MULTI-MODAL QCD

Observing the near-Gaussian mixture distributions with two modes in Fig. 2, we formulate the problem for the two-mode case. Our formulation can be naturally extended to an arbitrary number of modes.

### A. Overall Error Distribution

Let  $\epsilon$  denote the prediction error. Let  $f(\cdot)$  denote the overall error distribution of the training dataset, i.e., the empirical distribution function. For ease of exposition, we assume the training dataset is sufficiently large so that  $f$  can be treated as a probability density function (pdf). Let  $\mathcal{M} = \{0, 1\}$  denote the two possible modes, with 0 indicating low-error mode, and 1 indicating high-error mode. Suppose that  $f$  is a mixture distribution of two components, formally  $f(X) = \pi_0 f_0(X) + \pi_1 f_1(X)$ , where  $\pi_0 \geq 0$ ,  $\pi_1 \geq 0$ , and  $\pi_0 + \pi_1 = 1$ . The supports of  $f_0$  and  $f_1$  may overlap with each other. For example, when  $f$  is Gaussian mixture, the supports of  $f_0$  and  $f_1$  are both the entire  $\mathbb{R}$ . Without loss of generality, we assume  $\mathbb{E}_{\epsilon \sim f_0}[\epsilon] < \mathbb{E}_{\epsilon \sim f_1}[\epsilon]$ .

### B. Mode Dynamics

Let  $M_t \in \mathcal{M}$  denote the latent error mode at time  $t$ . The mode is *unobservable* and its *temporal evolution is unknown a priori*. In the real world, under the same overall error distribution  $f$ , there can be a wide range of mode dynamics. Some representative examples are as follows.

(i) *Static.* The mode  $M_t$  remains in a constant state  $m^*$  for extended durations, satisfying  $P(M_t = M_{t-1}) \approx 1$ . With

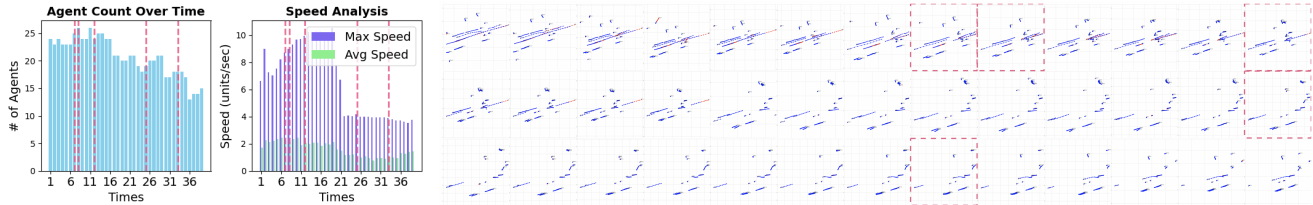


**Fig. 4: Observable scene-level information provides unreliable cues for error modes and their transitions.** The figure illustrates (i) agent counts over time, (ii) maximum and average speeds over time, and (iii) corresponding map snapshots of the driving scenes. The pink dashed lines indicate where a mode switch occurs.

initial distribution  $\mathbb{P}(M_0 = 0) = \pi_0$ , this dynamic captures highly persistent behaviors—such as highway cruising in *NGSIM*—where state switches are infrequent.

(ii) *i.i.d. switching*.  $\mathbb{P}(M_t = m) = \pi_m$  for  $m \in \{0, 1\}$  and  $M_t$ 's are independent across time. This dynamic encodes memoryless fluctuations.

(iii) *Markovian*, i.e.,  $\mathbb{P}\{M_t | M_{t-1}, \dots, M_0\} = \mathbb{P}\{M_t | M_{t-1}\}$  for any  $t \geq 1$ . This dynamic formalizes temporally correlated transitions, which typically occur in structured urban scenes.

(iv) *Arbitrary deterministic*, where the evolution of  $M_t$  over time may not be described by any well-studied random processes. This dynamic is the most general, yet challenging and pessimistic setting. We conjecture that in many real-world traffic environments, the latent mode dynamics often exhibit exploitable structure over time rather than arbitrary.

By unifying these dynamics through the overall error distribution  $f$ , our framework captures the inherent diversity and evolution of real-world traffic while maintaining analytical rigor.

### C. OOD Detection as Change-point Detection

Let  $\{\epsilon_t\}_{t=1}^{\infty}$  denote the sequence of prediction errors. Let  $\gamma$  be the unknown time at which the ego vehicle enters an OOD scenario, triggering a distributional shift:

$$\epsilon_t \sim \begin{cases} f_t(\cdot), & t < \gamma \\ g(\cdot), & t \geq \gamma. \end{cases}$$

Here,  $f_t$  represents the ID density. When  $M_t = 0$ ,  $f_t = f_0$ , and  $f_t = f_1$  otherwise. The post-change distribution  $g(\cdot)$  represents the OOD density.

1) *Detection Objective*: For any detection algorithm, we denote by  $\tau$  the time it declares OOD. For robustness, we adopt Lorden's minimax criterion [22], and define the *Worst-Case Average Detection Delay (WADD)* as

$$\text{WADD}(\tau) = \sup_{t \geq 1} \text{ess sup} \mathbb{E}_t [(\tau - t + 1)^+ | \epsilon_1, \dots, \epsilon_{t-1}],$$

where  $(x)^+ = \max\{0, x\}$  and  $\mathbb{E}_t[\cdot]$  denotes the expectation when the change occurs at  $t$ .

False alarms are quantified by the *False Alarm Rate (FAR)* and its reciprocal, the *Mean Time to False Alarm (MTFA)*:

$$\text{FAR}(\tau) = \frac{1}{\mathbb{E}_{\infty}[\tau]}, \quad \text{MTFA}(\tau) = \mathbb{E}_{\infty}[\tau],$$

where  $\mathbb{E}_{\infty}$  denotes expectation under the null hypothesis (no change occurs).

2) *Classic CUSUM Procedure*: For the simplified setting where  $f_t = \tilde{f}$  is time-invariant, and both  $\tilde{f}$  and  $g$  are known, the classic CUSUM procedure [29] is optimal for minimizing WADD [21]. Intuitively, the test statistic  $S_t$  accumulates the log-likelihood ratio via

$$S_t = \max\left(0, S_{t-1} + \ln \frac{g(\epsilon_t)}{\tilde{f}(\epsilon_t)}\right), \quad S_0 = 0. \quad (1)$$

A change is declared at  $\tau = \inf\{t \geq 1 : S_t \geq b\}$ , where the threshold  $b$  is calibrated to satisfy the given MTFA constraint.

3) *Operational Knowledge Paradigms*: In real-world practice, the a priori knowledge of  $f_t$  and  $g$  can vary. Oftentimes, the overall error distribution  $f$  can be estimated from ID data. Hence, we assume  $f$  is known. We consider multiple knowledge settings for the post-change distributions, following [1].

**Setting I: Full Knowledge.** The post-change distribution is fully specified. This setting serves as a performance upper bound. In many applications,  $g$  may be approximated via domain knowledge, incident logs, or simulation

**Setting II: Partial Knowledge.** When only coarse statistics of  $g$  (e.g., mean  $\mu_g$ , variance  $\sigma_g^2$ ) are available, we approximate  $g$  by  $\hat{g}(\epsilon) = \mathcal{N}(\epsilon | \mu_g, \sigma_g^2)$  and substitute into Eq. (1). This approximation remains valid as long as the log-likelihood ratio has negative drift before the real chance and positive drift after the real chance.

**Setting III: Unknown Knowledge.** When no parametric form of  $g$  is available, we adopt the robust shift-based CUSUM. The post-change distribution is approximated as a location-shifted version of the pre-change density,  $f(\epsilon - \kappa)$ , where  $\kappa > 0$  is a user-specified *minimum detectable shift*. The corresponding CUSUM statistic is:

$$S_t^{(\kappa)} = \max\left(0, S_{t-1}^{(\kappa)} + \log \frac{f(\epsilon_t - \kappa)}{f(\epsilon_t)}\right).$$

As shown in [1], this formulation guarantees valid false-alarm control for any true shift  $\eta \geq \kappa$ . The parameter  $\kappa$  should therefore be set conservatively small: underestimating  $\kappa$  preserves correctness at the cost of higher detection delay, whereas overestimating it (i.e.,  $\kappa > \eta$ ) can cause the detector to fail entirely. Following the guidelines in [1] and for fair comparison, we set  $\kappa = 1$  in all subsequent experiments.

### D. Prediction Error Metrics

In trajectory prediction,  $\epsilon_t$  may be defined in different ways depending on the chosen evaluation metric. We adopt three standard metrics [30]:

- *Average Displacement Error (ADE)*: mean  $\ell_2$  distance between predicted and ground-truth positions across the prediction horizon.
- *Final Displacement Error (FDE)*:  $\ell_2$  distance at the final prediction step, highlighting long-horizon accuracy.
- *Root Mean Squared Error (RMSE)*: square root of the average squared deviation, which penalizes large errors and is sensitive to outliers or abrupt shifts.

## V. METHOD

We propose *Mode-Aware CUSUM* (MA-CUSUM, Algorithm 1), an adaptive multi-threshold change-point detector that explicitly conditions on the latent error mode.

### A. MA-CUSUM

Algorithm 1 processes the prediction error stream  $\epsilon_1, \epsilon_2, \dots$  sequentially in three steps per time step.

1) *Mode Estimation*: We use Maximum A Posteriori (MAP) for mode estimation. Both GMM modes share overlapping support (Fig. 2), so we use soft probabilistic assignment via the posterior:  $P(M_t=m | \epsilon_t) = \pi_m f_m(\epsilon_t) / f(\epsilon_t)$ , with  $\hat{M}_t = \arg \max_m P(M_t=m | \epsilon_t)$ .

At each step, mode estimation uses only  $\epsilon_t$  with  $O(1)$  computation, and is strictly online without relying on future observations. MAP is the Bayes-optimal classifier under arbitrary yet deterministic mode dynamics [31], requiring no assumptions about transition structure. In addition, our adaptive threshold (Step 2) further tolerates occasional misclassification via conservative parameters ( $r_0 > r_1$ ).

2) *Adaptive Threshold Update*: The local error variance  $\hat{\sigma}^{(\hat{M}_t)}$  is estimated over a sliding window comprising the most recent  $L$  time steps where the estimated mode was  $\hat{M}_t$ . Specifically, let  $\mathcal{I}_t = \{\tau \leq t : \hat{M}_\tau = \hat{M}_t\}$  be the set of indices with matching mode estimates; the variance is computed over the  $L$  largest indices in  $\mathcal{I}_t$ . This yields a mode-specific scale  $d_{\hat{M}_t} = r_{\hat{M}_t} \hat{\sigma}^{(\hat{M}_t)}$ , which determines the SPRT-derived base threshold [22], [18]:  $h_{\hat{M}_t} = \frac{2}{d_{\hat{M}_t}^2} \ln\left(\frac{1-\beta_{\hat{M}_t}}{\alpha_{\hat{M}_t}}\right)$ , where  $\alpha_m$  and  $\beta_m$  control false alarm and missed detection rates. Scaling by variance makes the threshold more conservative when errors are volatile. Setting  $r_0 > r_1$  gives the low-error mode a higher threshold, absorbing transient mode fluctuations. The threshold is smoothed as  $\theta_t^{(\hat{M}_t)} = \lambda h_{\hat{M}_t} + (1-\lambda)\theta_{t-1}^{(\hat{M}_t)}$ , where  $\lambda$  controls tracking speed.

3) *CUSUM Update and Detection*: At each step, the log-likelihood ratio  $\ell_t$  quantifies shift evidence based on the knowledge paradigm: in **Setting I**,  $\ell_t = \ln(g/f_{\hat{M}_t})$ ; in **Setting II**,  $\ell_t = \ln(\mathcal{N}(\mu_g, \sigma_g^2)/f_{\hat{M}_t})$  using a Gaussian surrogate; and in **Setting III**,  $\ell_t = \ln(f_{\hat{M}_t}(\epsilon_t - \kappa)/f_{\hat{M}_t})$  with shift  $\kappa = 1$  [1]. The CUSUM statistic accumulates this evidence via  $S_t^{(\hat{M}_t)} = \max(S_{t-1}^{(\hat{M}_t)} + \ell_t - k_{\hat{M}_t}, 0)$ , where the drift correction  $k_{\hat{M}_t} = d_{\hat{M}_t}/2$  penalizes uncertainty and controls false alarms. A change is declared when  $S_t^{(\hat{M}_t)} \geq \theta_t^{(\hat{M}_t)}$ .

### Algorithm 1: Mode-Aware CUSUM (MA-CUSUM)

---

**Input:** Pre-change GMM  $(\pi_0, \pi_1, f_0, f_1)$ ;  
Knowledge  $\mathcal{K} \in \{\text{FULL, PARTIAL, UNKNOWN}\}$  with post-change specifications:  $g(\cdot)$  if  $\mathcal{K} = \text{Full}$ ;  $(\mu_g, \sigma_g^2)$  if  $\mathcal{K} = \text{Partial}$ .  
Tuning:  $(b_m, r_m, \alpha_m, \beta_m)_{m \in \{0,1\}}$ , window  $L$ , smoothing  $\lambda$ ;  
**Output:** Change point  $\tau$

---

```

Init.  $S_0^{(m)} \leftarrow 0$ ;
 $\theta_0^{(m)} \leftarrow b_m$  for  $m \in \{0,1\}$ ;
for  $t = 1, 2, \dots$  do
  Compute prediction error  $\epsilon_t$ ;
  /* Step 1: Mode estimation (MAP) */
   $\hat{M}_t \leftarrow \arg \max_{m \in \{0,1\}} \pi_m f_m(\epsilon_t)$ ;
  /* Step 2: Adaptive threshold */
  Estimate  $\hat{\sigma}^{(\hat{M}_t)}$  over window  $L$ ;
   $d_{\hat{M}_t} \leftarrow r_{\hat{M}_t} \hat{\sigma}^{(\hat{M}_t)}$ ;
   $h_{\hat{M}_t} \leftarrow \frac{2}{d_{\hat{M}_t}^2} \ln\left(\frac{1-\beta_{\hat{M}_t}}{\alpha_{\hat{M}_t}}\right)$ ;
   $\theta_t^{(\hat{M}_t)} \leftarrow \lambda h_{\hat{M}_t} + (1-\lambda)\theta_{t-1}^{(\hat{M}_t)}$ ;
  /* Step 3: Knowledge-aware LLR */
  if  $\mathcal{K} = \text{FULL}$  then // Setting I
     $\ell_t \leftarrow \ln \frac{g(\epsilon_t)}{f_{\hat{M}_t}(\epsilon_t)}$ 
  else if  $\mathcal{K} = \text{PARTIAL}$  then // Setting II
     $\ell_t \leftarrow \ln \frac{\mathcal{N}(\epsilon_t | \mu_g, \sigma_g^2)}{f_{\hat{M}_t}(\epsilon_t)}$ 
  else // Setting III
     $\ell_t \leftarrow \ln \frac{f_{\hat{M}_t}(\epsilon_t - \kappa)}{f_{\hat{M}_t}(\epsilon_t)}$ 
  /* Step 4: CUSUM update */
   $S_t^{(\hat{M}_t)} \leftarrow \max(S_{t-1}^{(\hat{M}_t)} + \ell_t - d_{\hat{M}_t}/2, 0)$ ;
  if  $S_t^{(\hat{M}_t)} \geq \theta_t^{(\hat{M}_t)}$  then return  $\tau = t$ ;

```

---

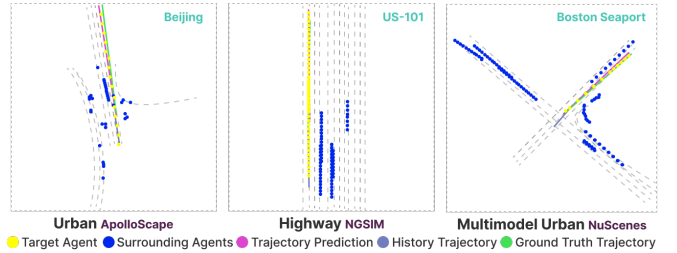


**Fig. 5: Three evaluation datasets:** ApolloScope (dense urban interactions), NGSIM (freeway driving), and nuScenes (multimodal urban scenes).

## VI. EXPERIMENTS

### A. Experimental Setup

We evaluate our MA-CUSUM across datasets and models chosen for diversity in traffic, interactions, sensing, and architecture:

**Datasets.** - *ApolloScope (Urban)* [26]. Urban traffic in Beijing, with dense mixed agent interactions (vehicles, pedestrians, riders), annotated trajectories from 1-minute camera/LiDAR sequences. High variability in interactions makes it suitable for testing rapid mode transitions.

- *NGSIM (Highway)* [27]. Freeway datasets (e.g. I-80, US-101) with long stretches of steady motion interspersed with lane changes or merges. Good for evaluating detection under mostly stable modes.

- *nuScenes (Multimodal Urban)* [28]. Urban driving in Boston and Singapore, full sensor coverage (cameras, Li-

**TABLE II:** OOD detection results (mean  $\pm$  std.) on GRIP++ and FQA. Our **MA-CUSUM** achieves the best **AUROC** (ranking accuracy) and **AUPR** (precision–recall robustness under class imbalance), consistently surpassing all baselines. Compared to Global CUSUM [1], it also produces markedly fewer false positives at high recall.

Method		GRIP++		FQA	
		AUROC	AUPR( $10^{-1}$ )	AUROC	AUPR( $10^{-1}$ )
<i>Likelihood-based</i>	IGMM [12]	$0.78 \pm 0.01$	$0.31 \pm 0.02$	$0.81 \pm 0.00$	$0.37 \pm 0.01$
	NLL [15]	$0.48 \pm 0.00$	$0.08 \pm 0.00$	$0.53 \pm 0.01$	$0.18 \pm 0.00$
<i>Sequential</i>	Z-Score [32]	$0.72 \pm 0.01$	$0.29 \pm 0.02$	$0.75 \pm 0.01$	$0.34 \pm 0.02$
	Chi-Square [33]	$0.76 \pm 0.01$	$0.34 \pm 0.02$	$0.78 \pm 0.01$	$0.40 \pm 0.02$
	Global CUSUM [1]	$0.87 \pm 0.01$	$0.53 \pm 0.07$	$0.89 \pm 0.01$	$0.76 \pm 0.08$
	<b>MA-CUSUM(ours)</b>	<b><math>0.93 \pm 0.01</math></b>	<b><math>1.11 \pm 0.14</math></b>	<b><math>0.95 \pm 0.01</math></b>	<b><math>1.95 \pm 0.17</math></b>

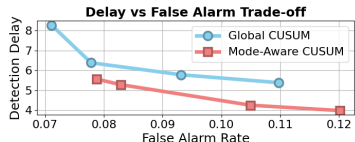


**Fig. 6:** Detection delay versus false alarm rate. Lower values on both axes indicate better performance (faster detection, fewer false alarms). MA-CUSUM (Red) shifts the trade-off curve toward the lower-left relative to Global CUSUM (Blue), achieving shorter detection delays at the same or lower false alarm rates.

**TABLE III:** Trajectory Prediction Vulnerability: ID vs. OOD performance across ADE, FDE, and RMSE. All metrics exhibit significant degradation under single-frame adversarial shifts.

Model	Dataset	ADE [m]			FDE [m]			RMSE [m]		
		ID	OOD	$\Delta\%$	ID	OOD	$\Delta\%$	ID	OOD	$\Delta\%$
GRIP	Apollo	1.97	7.14	+262	3.42	12.48	+265	2.45	8.94	+264
	NGSIM	7.29	9.24	+27	11.20	14.34	+28	8.81	11.36	+29
	nuSc.	5.46	8.32	+52	8.54	13.15	+54	6.63	10.25	+54
FQA	Apollo	2.37	5.64	+138	4.15	9.88	+138	3.02	7.18	+137
	NGSIM	5.44	7.05	+30	9.62	12.60	+31	7.15	9.38	+31
	nuSc.	5.28	7.83	+48	8.25	12.21	+48	6.55	9.72	+48

DAR, radar), many object types, varied environmental conditions. Useful for handling sensor uncertainty and interaction stochasticity.

**Model Selection.** - *GRIP++* [24]. A graph-based, two-layer GRU model that excels on short and long horizon forecasts. We adopt a distance threshold  $D_{\text{close}} = 25$  feet as in the original work to filter out distant agents.

- *FQA* [25]. Uses fuzzy attention integrating fuzzy rules with learned attention weights, allowing adaptive weighting of agent interactions. Suitable for complex urban scenes like nuScenes.

### B. OOD Data Generation

Evaluating runtime OOD detection requires realistic distribution shifts with known change points. We adopt the physically-constrained adversarial attack framework of [13] to generate OOD samples. This approach perturbs observed trajectories while respecting vehicle kinematics and scene constraints, yielding shifts that are subtle yet capable of inducing large prediction errors—a realistic proxy for safety-critical degradation. Unlike synthetic noise or manual trajectory editing, these adversarial perturbations preserve scene semantics and traffic interaction structure, producing challenging but physically plausible distribution shifts.

We apply perturbations starting at a predefined time, giving us precise ground-truth change points for evaluating detection delay (WADD) and false-alarm metrics without the ambiguity of naturally occurring drift. Table III summarises the impact of adversarial perturbations on prediction accuracy across three datasets and representative models, confirming that the generated OOD data induces substantial and consistent performance degradation.

### C. Main Results

Unless stated, experiments use Setting I as a performance upper bound. Table V demonstrates that while detection delay and AUROC degrade gracefully as knowledge diminishes, false-alarm control remains stable across all paradigms.

#### RQ1: Does mode-awareness improve OOD detection compared to likelihood-based and sequential baselines?

As shown in Table II, our method consistently outperforms all likelihood-based baselines (IGMM [12], NLL [15]), sequential detectors (Z-Score [32] and Chi-Square [33]), and Global CUSUM [1]. On GRIP++, MA-CUSUM achieves 0.93 AUROC and 1.11 AUPR( $\times 10^{-1}$ ), improving over Global CUSUM (0.87 / 0.53) by 7.2% in AUROC and 110.6% in AUPR. On FQA the gains are even larger: 0.95 vs. 0.89 AUROC (+6.6%) and 1.95 vs. 0.76 AUPR ( $\times 10^{-1}$ , +157.6%). The large AUPR gains show that multi-mode scoring is especially effective at reducing false positives when OOD events are rare. Overall, conditioning the sequential test on mode-specific error distributions consistently outperforms a single aggregate model in both ranking accuracy and precision.

#### RQ2: Does multi-mode improve the delay–false-alarm trade-off to single-distribution CUSUM?

Beyond overall performance (RQ1), we examine whether decomposing the detection statistic by mode is necessary when prediction errors exhibit mode-dependent heterogeneity. Classical CUSUM assumes a single stationary pre-change distribution. When traffic contains multiple behavioural modes (as stated in Section III), a single calibration induces a structural trade-off: conservative thresholds delay detection of hazardous transitions, whereas aggressive thresholds inflate false alarms during benign intra-mode variability. Fig. 6 shows that multi-mode consistently achieves lower detection delay at fixed

**TABLE IV:** Global vs. Mode-Aware CUSUM under four switching dynamics. WADD ( $\downarrow$ ) and  $\log_{10}(\text{MTFA})$  ( $\uparrow$ ) are averaged over 5000 runs with matched thresholds.

Dynamic	Global		Mode-Aware		Improvement	
	WADD $\downarrow$	$\log_{10}(\text{MTFA})$	WADD $\downarrow$	$\log_{10}(\text{MTFA})$	$\Delta\text{WADD}$ (%)	$\Delta\text{MTFA}$ (%)
Static	12.30	3.45	11.80	3.48	4.10	8.90
Markov	18.70	3.08	11.20	3.35	40.10	87.50
Arbitrary	17.20	3.13	12.00	3.39	30.20	81.50
i.i.d.	13.80	3.26	12.90	3.41	14.60	41.70

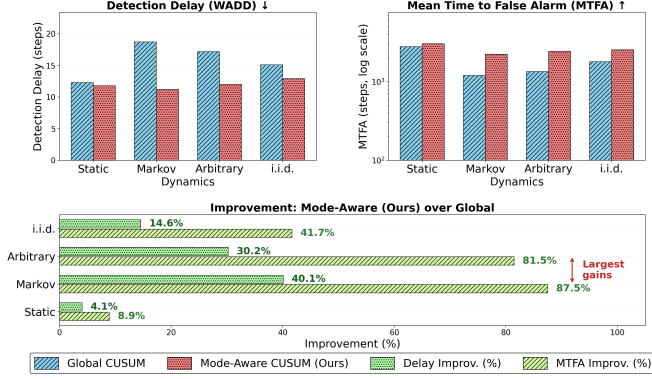


**Fig. 7: Detection performance (delay vs. false-alarm rate) of Global CUSUM and Mode-Aware CUSUM under Markov, i.i.d., static, and arbitrary mode-switching models.** Synthetic trajectories are generated by GRIP++ across the three datasets in Section VI-A (sequence length  $T = 3000$  steps, averaged over  $N = 5000$  runs per configuration under a shared threshold  $h$ ).

false-alarm levels, with the largest gains in safety-relevant low-FAR regimes. The improvement arises because mode-aware log-likelihood ratios preserve local statistical power, whereas global averaging dilutes change evidence and enlarges the vulnerability window before alarm.

**RQ3: How do the switching dynamics between low-error and high-error regimes influence the statistical gains of multi-mode detection?** As summarized in Table IV, the performance gain of Mode-Aware CUSUM is heavily moderated by the temporal persistence of the underlying regimes. In *Markov* and *Arbitrary* dynamics—which most closely mirror real-world driving contexts—the method achieves a 30.2%–40.1% reduction in WADD. This confirms that when regimes persist, the benefit of regime-specific score functions outweighs the reduced update frequency per statistic. Conversely, the *Static* case yields a more modest 4.1% improvement. This result highlights the inherent trade-off between detector robustness and sensitivity. In an unchanging environment, the Mode-Aware machinery introduces a “tolerance overhead”: the MAP estimator’s sensitivity to stochastic noise near GMM component boundaries can trigger momentary mode-misassignments. Additionally, the parameters designed to stabilize the detector during transitions (e.g., threshold smoothing  $\lambda$  and conservative  $r_m$  values) act as a slight sensitivity penalty in the absence of actual switches. However, the fact that performance remains superior to the Global baseline even in the *Static* and *i.i.d.* cases demonstrates that the proposed framework is robust to a wide range of non-stationary behaviors without suffering from negative

**TABLE V:** Robustness under varying post-change knowledge. FAR remains stable; delay and AUROC degrade gracefully as assumptions weaken. The unknown-knowledge setting uses  $\kappa = 1$  (Section IV-C.3).

Knowledge	Log-likelihood ratio $\ell_t$	Delay $\downarrow$	FAR $\downarrow$	AUROC $\uparrow$
Setting I: Full	$\ln \frac{g(\epsilon_t)}{f_{\hat{M}_t}(\epsilon_t)}$	8.2	0.034	0.95
Setting II: Partial	$\ln \frac{\mathcal{N}(\epsilon_t   \mu g, \sigma g^2)}{f_{\hat{M}_t}(\epsilon_t)}$	9.1	0.036	0.93
Setting III: Unknown	$\ln \frac{f_{\hat{M}_t}(\epsilon_t - \kappa)}{f_{\hat{M}_t}(\epsilon_t)}$	12.4	0.035	0.895

**TABLE VI:** Computational cost comparison. Ensemble and MC-Dropout require multiple forward passes; our CUSUM variants add lightweight post-hoc monitoring atop a single pass.  $M$ : ensemble size,  $S$ : dropout samples,  $D$ : feature dimensions

Method	Fwd. Passes	Complexity	Time (ms)
Deep Ensemble	$M$	$O(M \cdot D)$	38.7
MC-Dropout	$S$	$O(S \cdot D)$	29.4
Global CUSUM(base)	1	$O(1)$	4.3
MA-CUSUM (ours)	1	$O(1)$	5.1

transfer in simpler scenarios.

**RQ4: How robust is multi-mode detection under imperfect post-change knowledge and limited observability?**

Classical CUSUM assumes a fully known post-change distribution  $g$ , yet real-world robotic deployment rarely affords this luxury. To quantify the impact of such uncertainty, we evaluate three operationally motivated knowledge settings (Section IV-C.3), ranging from ideal to worst-case. Table V reports results across all three settings. The key finding is that FAR remains stable regardless of post-change uncertainty—even under severe variance misspecification ( $\pm 50\%$   $\sigma$ ). Detection delay increases monotonically from the oracle baseline (8.2 steps) to the unknown setting (12.4 steps), while AUROC degrades gracefully from 0.948 to 0.894. This reliability arises because the framework anchors its safety guarantees on the pre-change model  $f_t$  rather than  $g$ . Consequently, the system is deployment-ready: it maintains reliable safety bounds while naturally translating better environment knowledge into faster detection.

*D. Further Discussions*

**Computational Efficiency.** We compare the computational demand of our method against common uncertainty baselines (Table VI). Ensemble and MC-Dropout methods require  $M$  or  $S$  full forward passes, whereas our multi-mode detector operates as a lightweight post-hoc layer on top of a

single predictor pass. Specifically, MA-CUSUM scales as  $O(1)$  maintaining comparable complexity as Global CUSUM while enabling the per-mode statistical decomposition that drives the detection gains reported above.

**Update Frequency and Deployment.** A potential concern is whether partitioning data across modes reduces per-mode sample counts, thus degrading detection quality. Our results demonstrate that per-mode threshold calibration effectively compensates for the reduced update rate by tightly matching each mode’s error distribution. Quantitatively, even in high-switching scenarios (Urban Intersections), MA-CUSUM maintains gains of  $> 35\%$ . These consistent improvements across diverse traffic environments—from residential corridors to dense urban intersections—indicate that the multi-mode sequential framework is practical for on-board deployment in production autonomous vehicles.

## VII. CONCLUSION

We introduced MA-CUSUM, a multi-mode change-point detector that leverages the modal structure of trajectory prediction errors for adaptive OOD detection. Unlike static or frame-wise baselines, MA-CUSUM maintains context-sensitive thresholds that balance sensitivity across diverse driving scenarios. Our results demonstrate that MA-CUSUM consistently outperforms classic baselines and existing UQ methods, achieving lower detection delay and fewer false alarms. This highlights that “one-size-fits-all” detection is inherently suboptimal: single thresholds are typically too sensitive in simple scenes or too conservative in complex ones. Future work will investigate downstream mitigation strategies once OOD is detected, such as safe fallback maneuvers or uncertainty-aware control. We also aim to incorporate heavy-tailed components (e.g., Student- $t$  mixtures) to better capture rare scenes.

## REFERENCES

- [1] T. Guo, T. Banerjee, R. Liu, and L. Su, “Building real-time awareness of out-of-distribution in trajectory prediction for autonomous vehicles,” *arXiv preprint arXiv:2409.17277*, 2024.
- [2] J. Nitsch, M. Itkina, R. Senanayake, J. Nieto, M. Schmidt, R. Siegwart, M. J. Kochenderfer, and C. Cadena, “Out-of-distribution detection for automotive perception,” in *2021 IEEE International Intelligent Transportation Systems Conference (ITSC)*, 2021, pp. 2938–2943.
- [3] Y. Shoeb, A. Nowzad, and H. Gottschalk, “Out-of-distribution segmentation in autonomous driving: Problems and state of the art,” in *Proceedings of the Computer Vision and Pattern Recognition Conference*, 2025, pp. 4310–4320.
- [4] D. Hendrycks and K. Gimpel, “A baseline for detecting misclassified and out-of-distribution examples in neural networks,” *arXiv preprint arXiv:1610.02136*, 2016.
- [5] W. Liu, X. Wang, J. Owens, and Y. Li, “Energy-based out-of-distribution detection,” *Advances in neural information processing systems*, vol. 33, pp. 21 464–21 475, 2020.
- [6] Y. Gal and Z. Ghahramani, “Dropout as a bayesian approximation: Representing model uncertainty in deep learning,” in *international conference on machine learning*. PMLR, 2016, pp. 1050–1059.
- [7] A. Nayak, A. Eskandarian, and Z. Doerzaph, “Uncertainty estimation of pedestrian future trajectory using bayesian approximation,” *IEEE Open Journal of Intelligent Transportation Systems*, vol. 3, pp. 617–630, 2022.
- [8] A. Zyner, S. Worrall, and E. Nebot, “A recurrent neural network solution for predicting driver intention at unsignalized intersections,” *IEEE Robotics and Automation Letters*, vol. 3, no. 3, pp. 1759–1764, 2018.
- [9] X. Li, X. Ying, and M. C. Chuah, “Grip: Graph-based interaction-aware trajectory prediction,” in *2019 IEEE Intelligent Transportation Systems Conference (ITSC)*. IEEE, 2019, pp. 3960–3966.
- [10] A. Postnikov, A. Gamayunov, and G. Ferrer, “Transformer based trajectory prediction,” *arXiv preprint arXiv:2112.04350*, 2021.
- [11] Z. Wang, G. Zhang, T. Sun, C. Shi, and B. Zhou, “Data-driven methods for low-dimensional representation and state identification for the spatiotemporal structure of cavitation flow fields,” *Physics of fluids*, vol. 35, no. 3, 2023.
- [12] J. Wiederer, J. Schmidt, U. Kressel, K. Dietmayer, and V. Belagiannis, “Joint out-of-distribution detection and uncertainty estimation for trajectory prediction,” in *2023 IEEE/RSJ International Conference on Intelligent Robots and Systems (IROS)*. IEEE, 2023, pp. 5487–5494.
- [13] Q. Zhang, S. Hu, J. Sun, Q. A. Chen, and Z. M. Mao, “On adversarial robustness of trajectory prediction for autonomous vehicles,” in *Proceedings of the IEEE/CVF Conference on Computer Vision and Pattern Recognition*, 2022, pp. 15 159–15 168.
- [14] J. Wiederer, J. Schmidt, U. Kressel, K. Dietmayer, and V. Belagiannis, “Joint out-of-distribution detection and uncertainty estimation for trajectory prediction,” in *2023 IEEE/RSJ International Conference on Intelligent Robots and Systems (IROS)*, 2023, pp. 5487–5494.
- [15] K. Lee, K. Lee, H. Lee, and J. Shin, “A simple unified framework for detecting out-of-distribution samples and adversarial attacks,” *Advances in neural information processing systems*, vol. 31, 2018.
- [16] P. Cui and J. Wang, “Out-of-distribution (ood) detection based on deep learning: A review,” *Electronics*, vol. 11, no. 21, p. 3500, 2022.
- [17] Y. Sun, Y. Ming, X. Zhu, and Y. Li, “Out-of-distribution detection with deep nearest neighbors,” in *International Conference on Machine Learning*. PMLR, 2022, pp. 20 827–20 840.
- [18] V. V. Veeravalli and T. Banerjee, “Quickest change detection,” in *Academic press library in signal processing*. Elsevier, 2014, vol. 3, pp. 209–255.
- [19] A. G. Tartakovsky, A. S. Polunchenko, and G. Sokolov, “Efficient computer network anomaly detection by changepoint detection methods,” *IEEE Journal of Selected Topics in Signal Processing*, vol. 7, no. 1, pp. 4–11, 2012.
- [20] A. Tartakovsky, I. Nikiforov, and M. Basseville, *Sequential analysis: Hypothesis testing and changepoint detection*. nill: CRC press, 2014.
- [21] G. V. Moustakides, “Optimal stopping times for detecting changes in distributions,” *the Annals of Statistics*, vol. 14, no. 4, pp. 1379–1387, 1986.
- [22] G. Lorden, “Procedures for reacting to a change in distribution,” *The annals of mathematical statistics*, pp. 1897–1908, 1971.
- [23] B. Hajek, *Random processes for engineers*. Cambridge university press, 2015.
- [24] X. Li, X. Ying, and M. C. Chuah, “Grip++: Enhanced graph-based interaction-aware trajectory prediction for autonomous driving,” *arXiv preprint arXiv:1907.07792*, 2019.
- [25] N. Kamra, H. Zhu, D. K. Trivedi, M. Zhang, and Y. Liu, “Multi-agent trajectory prediction with fuzzy query attention,” *Advances in Neural Information Processing Systems*, vol. 33, pp. 22 530–22 541, 2020.
- [26] X. Huang, X. Cheng, Q. Geng, B. Cao, D. Zhou, P. Wang, Y. Lin, and R. Yang, “The apollo dataset for autonomous driving,” in *Proceedings of the IEEE conference on computer vision and pattern recognition workshops*. nill: nill, 2018, pp. 954–960.
- [27] Federal Highway Administration. (2020) Traffic analysis tools: Next generation simulation. nill. [Accessed: Sep. 13, 2024]. [Online]. Available: <https://ops.fhwa.dot.gov/trafficanalysis/tools/ngsim.htm>
- [28] H. Caesar, V. Bankiti, A. H. Lang, S. Vora, V. E. Liong, Q. Xu, A. Krishnan, Y. Pan, G. Baldan, and O. Beijbom, “nusenes: A multimodal dataset for autonomous driving,” in *Proceedings of the IEEE/CVF conference on computer vision and pattern recognition*. nill: nill, 2020, pp. 11 621–11 631.
- [29] E. S. Page, “Continuous inspection schemes,” *Biometrika*, vol. 41, no. 1/2, pp. 100–115, 1954.
- [30] H. Kim, D. Kim, G. Kim, J. Cho, and K. Huh, “Multi-head attention based probabilistic vehicle trajectory prediction,” in *2020 IEEE Intelligent Vehicles Symposium (IV)*, IEEE. nill: nill, 2020, pp. 1720–1725.
- [31] T. M. Cover, *Elements of information theory*. John Wiley & Sons, 1999.
- [32] W. A. Shewhart, *Economic Control of Quality of Manufactured Product*. D. Van Nostrand Company, 1931.
- [33] H. Hotelling, “Multivariate quality control,” *Techniques of Statistical Analysis*, pp. 111–184, 1947.